Supplementary material for Thrusts control the thermal maturity of accreted sediments

Utsav Mannu[1,*], David Fernández-Blanco[2], Ayumu Miyakawa[3], Taras Gerya[4], and Masataka Kinoshita[5]

[1]Discipline of Earth Sciences, Indian Institute of Technology, Gandhinagar, India

[2] Barcelona Center of Subsurface Imaging, Institut de Ciències del Mar (ICM-CSIC), Barcelona, Spain;

[3]Geological Survey of Japan, AIST

[4]Institute of Geophysics, ETH Zurich

[5]Earthquake Research Institute, UTokyo

Correspondence to: Utsav Mannu (utsav.mannu@iitgn.ac.in)

Contents

- Rheological model
- Boundary conditions
- Surface processes
- Limitations
- Initial model setup

- **List of supplementary figures**
  - Fig **S1-S7**

- **List of supplementary movies**
  - **M_0.1_12.mp4** (Evolution of Lithology for Model $M_{0.1}^{12}$)
  - **M_0.3_12.mp4** (Evolution of Lithology for Model $M_{0.3}^{12}$)
  - **M_0.5_12.mp4** (Evolution of Lithology for Model $M_{0.5}^{12}$)
  - **M_0.7_12.mp4** (Evolution of Lithology for Model $M_{0.7}^{12}$)
  - **M_0.9_12.mp4** (Evolution of Lithology for Model $M_{0.9}^{12}$)
  - **M_2_0.mp4** (Evolution of Lithology for Model M_0^2)
  - **M_7_0.mp4** (Evolution of Lithology for Model M_0^7)
  - **M_12_0.mp4** (Evolution of Lithology for Model M_0^{12})
  - **M_17_0.mp4** (Evolution of Lithology for Model M_0^{17})
  - **M_22_0.mp4** (Evolution of Lithology for Model M_0^{22})

Supplementary text

In our visco-plastic/brittle model with variable viscosity, finite conservative difference ensures conservation of stresses by harmonizing the formulation of deviatoric stress across adjacent nodes. The topographic boundary in the model is simulated by an adaptive irregular surface grid coupled to the thermomechanical grid. The surface processes applied to the model are primarily implemented on this grid and are realized through the conversion of rock markers to air/water markers across this boundary, and vice-versa. Surface grid nodes can also be advected horizontally and vertically using velocities interpolated from the thermomechanical grid. As a result, both tectonic forcing and surface processes can change the model topography. Most of the sedimentation in the model happens as a cascading deposition of sediments from sea to land in subsequent basins. A free-slip boundary condition is implemented on all boundaries, except for the lower one which remains permeable to ensure mass conservation. We set thermally insulating boundary conditions on all sides except the lower one where the external thermal boundary condition is implemented.

1. Governing equations

The mass conservation is described by the continuity equation with the Boussinesq approximation of incompressibility as:

$$\frac{\partial v_x}{\partial x} + \frac{\partial v_y}{\partial y} = 0 \qquad (eq.1)$$

The equation for conservation of momentum with an incompressibility assumption is expressed in the 2D- stokes equation, for the *x*-axis and *y*-axis, respectively, as follows:

$$\frac{\partial \sigma_{xx}}{\partial x} + \frac{\partial \sigma_{xy}}{\partial y} = \frac{\partial P}{\partial x} \qquad (eq.2)$$

$$\frac{\partial \sigma_{yy}}{\partial y} + \frac{\partial \sigma_{xy}}{\partial x} = \frac{\partial P}{\partial x} - g\rho(T, P, C, M) \qquad (eq.3)$$

Where density $g\rho(T, P, C, M)$ depends on temperature (*T*), pressure (*P*), composition (*C*), and mineralogy (*M*).

The thermal equation used in the model is as follows:

$$\rho C_P \frac{DT}{Dt} = -\frac{\partial q_x}{\partial x} - \frac{\partial q_y}{\partial y} + H_r + H_a + H_s + H_l \qquad (eq.4)$$

where,

$$q_x = -k(T,C)\frac{\partial T}{\partial x}, q_y = -k(T,C)\frac{\partial T}{\partial y} \qquad (eq.5)$$

$$H_a = T\alpha\frac{DP}{Dt}, H_s = \sigma_{xx}\dot{\varepsilon}_{xx} + \sigma_{yy}\dot{\varepsilon}_{yy} + \sigma_{xx}\dot{\varepsilon}_{xy} \qquad (eq.6)$$

Where $D/DT$is a lagrangian time derivative, and x and y denote the horizontal and vertical coordinates, respectively; $\sigma_{xx}, \sigma_{xy}, \sigma_{yy}$ are components of the deviatoric stress tensor; $\dot{\varepsilon}_{xx}, \dot{\varepsilon}_{yy}, \dot{\varepsilon}_{xy}$ are components of the strain rate tensor; P is pressure; T is temperature; $q_x$and q_y are the components of heat flux in the horizontal and vertical direction; ρ is density; $g$is the gravitational acceleration; $C_P$is the isobaric heat capacity; H_r, H_a, H_s, H_l, denote, the radioactive, adiabatic, shear and latent heat production, respectively. $k(T,C)$ is the thermal conductivity, a function of composition, depth, and temperature(Table 1). To match the empirical relationship between depth and thermal conductivity, as measured on core samples in the borehole at IODP Site C0002(Sugihara et al., 2014; H. Tobin et al., 2015). To simulate the decrease in thermal conductivity near the surface caused by increased porosity, we modify the thermal conductivity formulation for sediments as a function of temperature and depth as follows

$$k_{sed} = 0.96 + \frac{807}{T+77}(1 - e^{\frac{-Z^2}{1.3e^7}})$$

For décollement we again use a similar relationship however with a larger thermal conductivity near the surface to emulate higher heat transfer in shear zones due to fluid advection

$$k_{sed} = 1.5 + \frac{807}{T+77}(1 - e^{\frac{-Z^2}{1.3e^7}})$$

2. Rheological model

The expression for effective creep viscosities(η_{eff}) of the materials used in the model is determined from experimental data(Ranalli, 1995) using a calibrated parameterized function of pressure(P) and temperature(T), known as flow law (Table 1).

$$\eta_{eff} = F(\dot{\varepsilon}_{II})^{1-n} A_D{}^{\frac{-1}{n}} h^m exp\left(-\frac{E_a + V_a P}{nRT}\right) \qquad (eq.7)$$

where, F is a dimensionless constant that depends on the type of experiments used for calibration, P is pressure (Pa), T is the temperature (K), R is the gas constant (8.314 J/K/mol), h is grain size (m) and A_D, n, m, E_a and V_a are experimentally determined rheological parameters: A_D is the material constant ($Pa^{-n}s^{-1}m^{-m}$), n is the stress exponent, m is the grain size exponent, E_a is activation energy (J/mol) and V_a is activation volume (J/Pa). As dislocation creep does not depend on grain size therefore we assume $h^m = 1$. $\dot{\varepsilon}_{II}$ is the second invariant of strain tensor computed as

$$\dot{\varepsilon}_{II} = \sqrt{\frac{\dot{\varepsilon}_{ij} * \dot{\varepsilon}_{ij}}{2}} \qquad (eq.8)$$

The model uses visco-plastic rheology to account for both brittle rheology of the shallower and colder rigid lithosphere and deeper, hotter ductile lithosphere and asthenosphere. Using the Mohr-Coulomb failure criterion we limit effective viscosity as

$$\eta_{eff} \leq \frac{c + Psin(\varphi)}{2\dot{\varepsilon}_{II}} \qquad (eq.9)$$

Where, c is cohesion and φ is an effective internal angle of friction or $\mu = tan(\varphi)$ where $\mu$is the coefficient of internal friction.

3. Boundary conditions

A free-slip boundary condition is implemented on all boundaries, except on the lower boundary, where is passable in the vertical direction. Where we implement, an external free slip condition similar to (Burg & Gerya, 2005) where a free slip condition is satisfied at an external boundary such that

$$\frac{\partial V_x}{\partial x} = 0, \frac{\partial V_y}{\partial y} = \frac{V_y}{\Delta Y_{external}} \qquad (eq.16)$$

Where, V_x and V_y, are the velocities in the horizontal and vertical directions at the boundary, $\Delta Y_{external}$ is the depth that lies outside the modeling domain, and where free slip condition is maintained. Similarly, we set thermally insulating boundary conditions on all sides except the lower one where the external thermal boundary condition is implemented.

4. Surface processes

The rock-water/air boundary is simulated by an adaptive irregular grid that is advected horizontally and vertically and is coupled to the thermomechanical grid which controls the tectonic change of the surface. Apart from the tectonic changes, surface processes prescribed in the model can also change the topography. The surface process in the model is controlled by conversion of rock markers to air/water and vice versa. All sedimentation in the model happens as a focused deposition of sediments from sea to land in morphological depressions (e.g. trench) is modelled as follows (Figure S2)

$$Y_{new} = Y_{old} + K \bullet Y_{fill} \qquad (eq.10)$$

Where, $K = min\left(\frac{V_{budget}}{V_{basin}}, 1\right)$

Due to the arbitrary shape of the basin, filling the basin using the above equation can overfill /underfill in a specific step. However, we compute the volume of the sediments that have been deposited and balance out the sediment deficit/overfill in the next step. Therefore over long run the sedimentation amount remains equivalent to the prescribed amount.

5. Limitations

For instance, even with a minimum grid size of 150 m x 500 m, the model is not able to simulate very narrow faults that usually occur in nature and lead to a very local increase in thermal maturity. Therefore, while the thermal maturity anomaly observed in the borehole can be concentrated at the site of the fault which can be only a few centimeters wide, thermal maturity for our model can be spread over several hundred meters (Fig. 7). Wider faults also result in a smaller characteristic time for local heat diffusion, meaning the rise in temperature due to viscous heating in faults is sustained for a smaller period. Consequently, in our models, the relative rise in thermal maturity of sediments in faults is far less compared to the observations in the borehole. This problem could be resolved in the future using adaptive gridding, where one can temporarily increase the resolution in zones with high strain rates, leading to much narrower faults and concentrated elevation of heat and maturity in faults.

Another assumption in our model is that the model does not contain compaction or an increase in sediment strength with increasing depth and thickness of the wedge. Although this was done to keep the model simple, in the future one can introduce an empirical increase in material strength both with depth and seaward to landward.

Additionally, thermal maturity which is related to porosity by (Schmoker & Gautier, 1988) can also be used to give a measure of compaction in the wedge and could be linked to material strength. However, one needs to be careful while implementing this relationship as fault zones which generally have a higher thermal maturity due to viscous heating tend to have lower strength. We have also not considered the influence of fluid flow in our models, which can have a significant impact on the maturity value, especially in the fault zones. However, to mimic this effect we used elevated values of conductivity for the weak material present in the décollement.

6. Initial model setup

The modelling domain is 3500 km wide and 350 km deep and is discretized into 1284 × 401 nodes populated with ~25 million markers. At the site of accretionary wedge evolution, we assign a significantly higher resolution of 130 m (vertical) × 300 m (horizontal), which steadily decreases near the boundary of the modelling domain. The simulation consists of an oceanic plate converging with a velocity of ~5 cm/yr and subducting beneath the continental plate (see Fig. S1). The oceanic plate consists of a 1-km-thick upper oceanic crust and a 7-km-thick lower oceanic crust underlain by a 47-km-thick mantle lithosphere. We use a thin (10 km) "sticky air" layer to overlay the top face of the rock strata inside the model which is a fluid with a low viscosity of 5E+17 Pa.s. and a low density, similar to air (white in Figure S1) or water (light blue in Figure S1). Displacement along the megathrust, at the contact between subducting oceanic plate and the overriding continental plate, occurs in a relatively weak basal layer in accretionary wedges across the globe(Byrne & Fisher, 1990). We simulate this with a predefined configuration at the interplate, with a 350-meter-thick décollement below a 1km thick sediment layer. The wedge forms above this interphase by accretion of sediments against the continental plate. The continental plate consists of an upper and lower continental crust with thicknesses of~ 20 km and ~15 km, respectively, and underlain by a mantle lithosphere of ~25 km. The transition between the lithosphere and asthenosphere is prescribed to occur at 1300°C. A weak layer is emplaced at the junction of both plates, which fails mechanically and leads to subduction initiation. Please refer to Table 1 for the rheological and thermal properties of all the materials used.

List of supplementary figures.

Fig. S1:*Initial model setup.* ***A.*** *The lithological and geothermal map of the whole computational domain with boundary conditions.* ***B.*** *The zoomed lithological and geothermal map of the inset illustrates the junction of continental and oceanic plates. The colors represent different lithology of the materials used in the models, with upper and lower crust represented by light and dark grey, upper and lower oceanic crust represented by dark and light green. The arrows around the computational domain represent the imposed boundary conditions, while the white contour lines(dashed in the zoomed panel) show the geothermal gradients used for the initial model. The numbers on the white contour lines represent the temperature values in °C for the contour.*

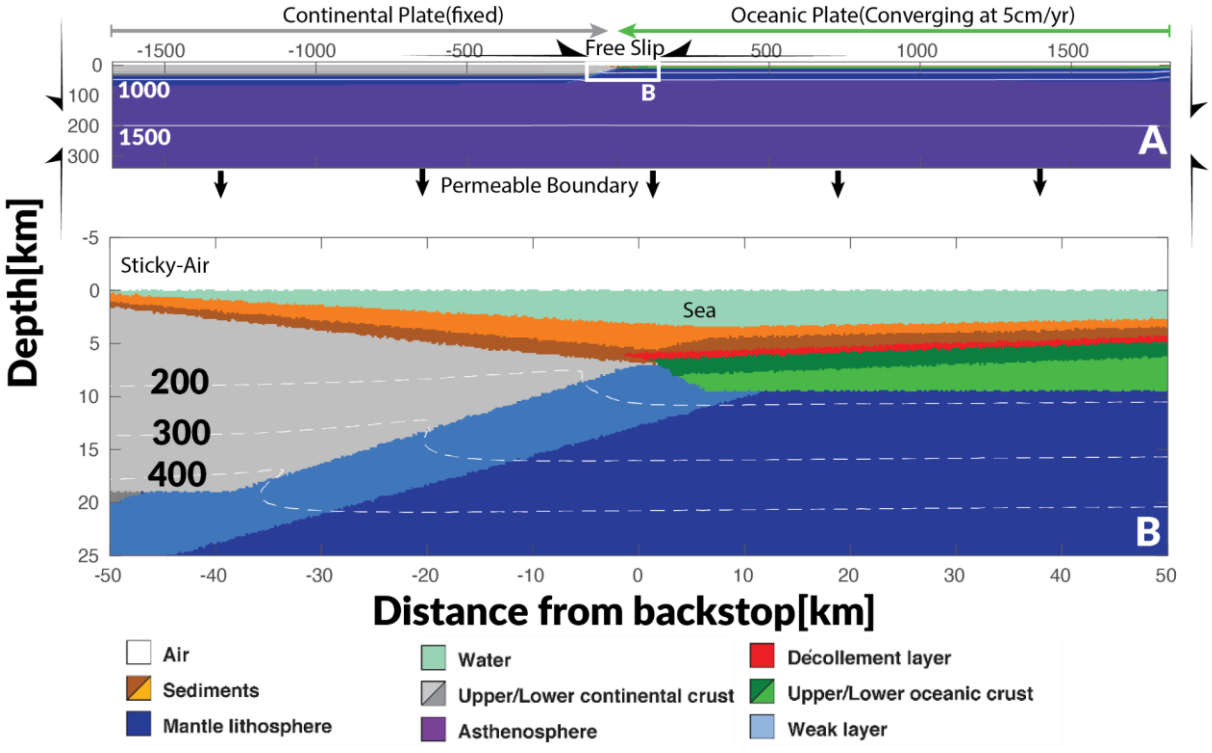

175 ***Fig S2:*** *Scheme of trench sedimentation in models (taken from (Mannu et al., 2017))*

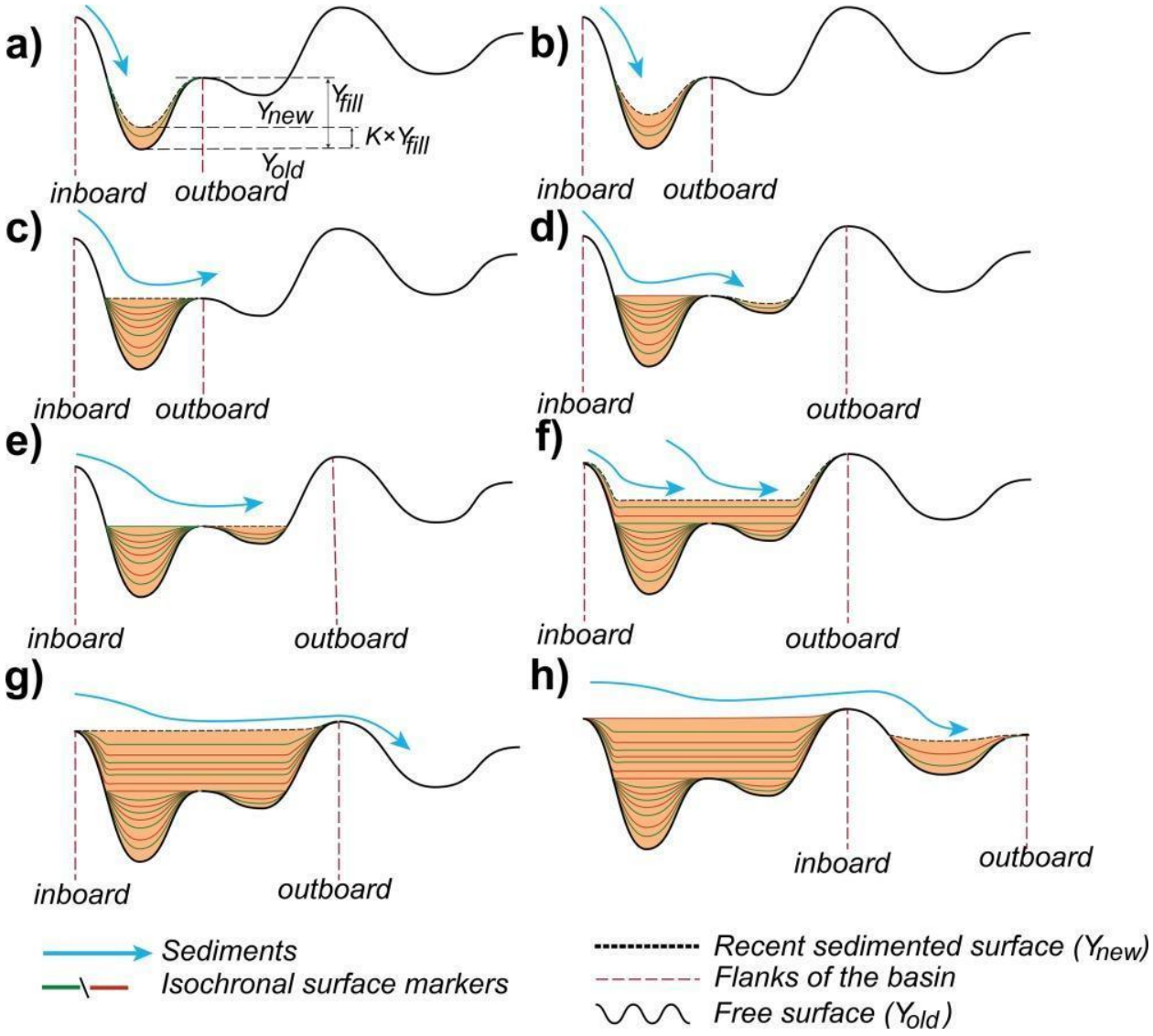

176

177

Fig. S3: *Plot of Temperature vs Depth profile in for water-sediment interaction using the data from the International Argo Program and the national programs that contribute for the location(represented by the white square) given in the inset. The magenta circle represent the Temperature vs Depth profile from the data while the black line is the fitted thermocline used in our models for water-sediment thermal interaction.*

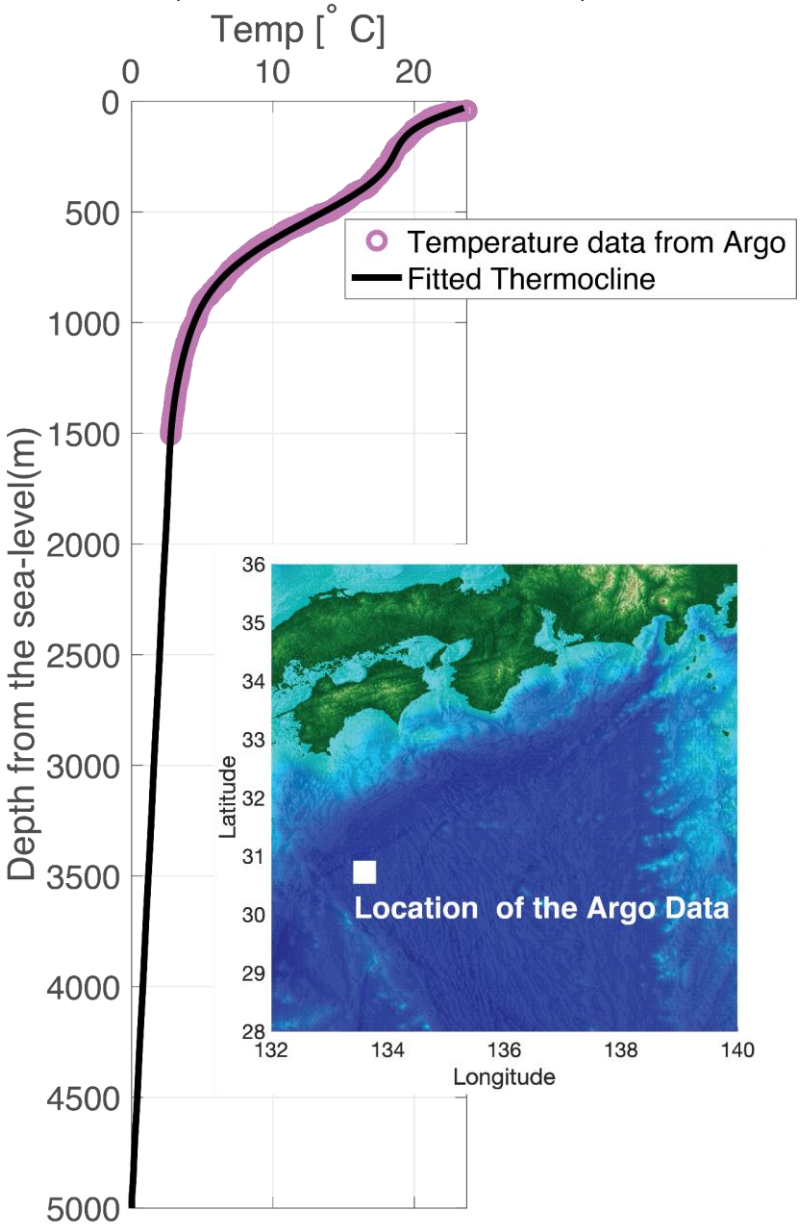

Fig. S4: *Plot of Temperature vs Depth profile in all models compared to Temperature-depth profile based on in-situ temperature from the long-term borehole monitoring system (indicated red patch is the range of temperature estimated by (Sugihara et al., 2014))*

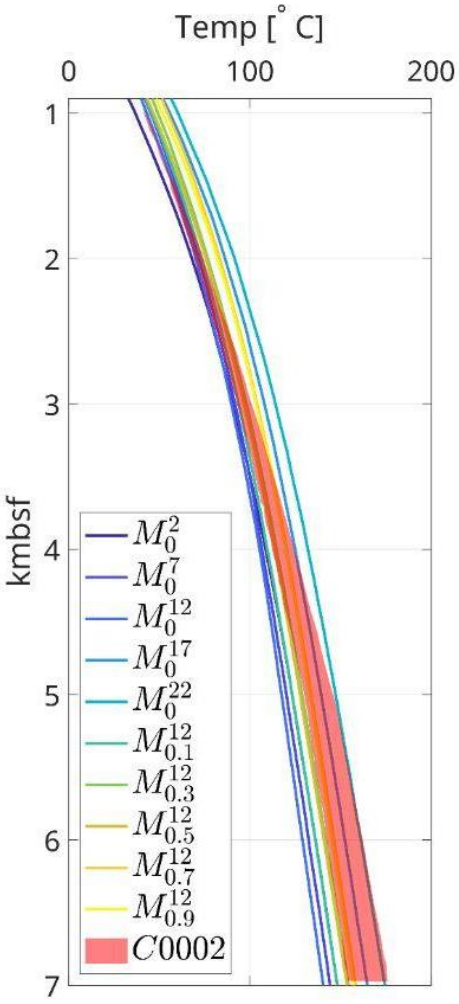

Fig. S5 *Trajectory of sediments in model . The wedge on top shows the location of individual boreholes relative to the position of the trench at 2.5 Myr. In each borehole, A-L 10 points are plotted for their trajectories between 2.5 Myr and 7.5 Myr. The color of markers in the trajectories represent the evolution of thermal maturity on individual sediment markers while undergoing evolution.*

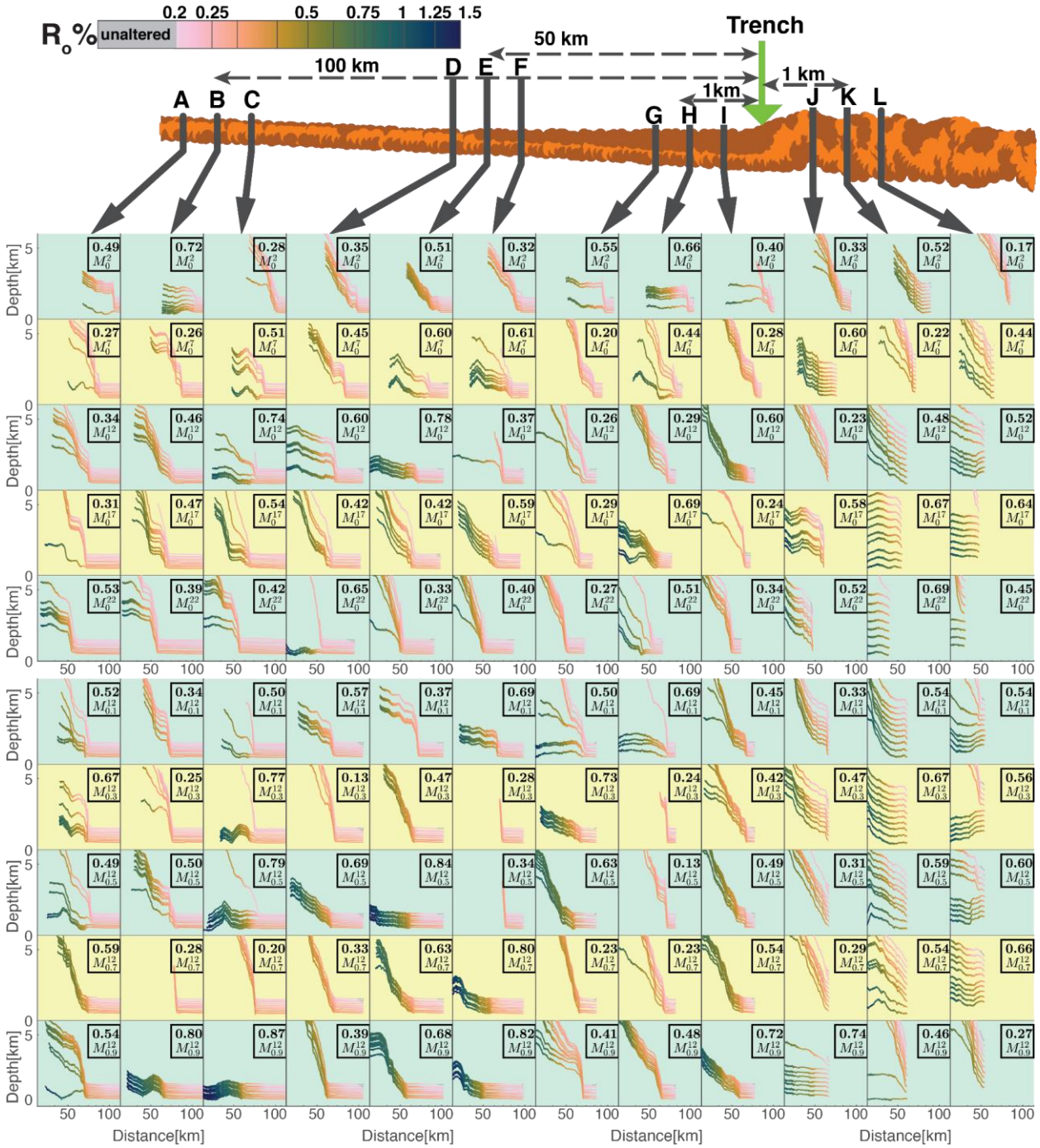

Fig. S6 *Vitrinite Reflectance(**%R₀**) vs Maximum Exposure temperature in models. Panel A,B and C show the Temperatures as a function of **%R₀** computed from Easy%R_0 , Simple%R_0 , Basin%R_0 for models* M_0^2-M_0^{22} . *Similarly panels D,E and F show the Temperatures as a function of **%R₀** computed from Easy%R_0 , Simple%R_0 , Basin%R_0 for models* $M_{0.1}^{12}$-$M_{0.9}^{12}$.

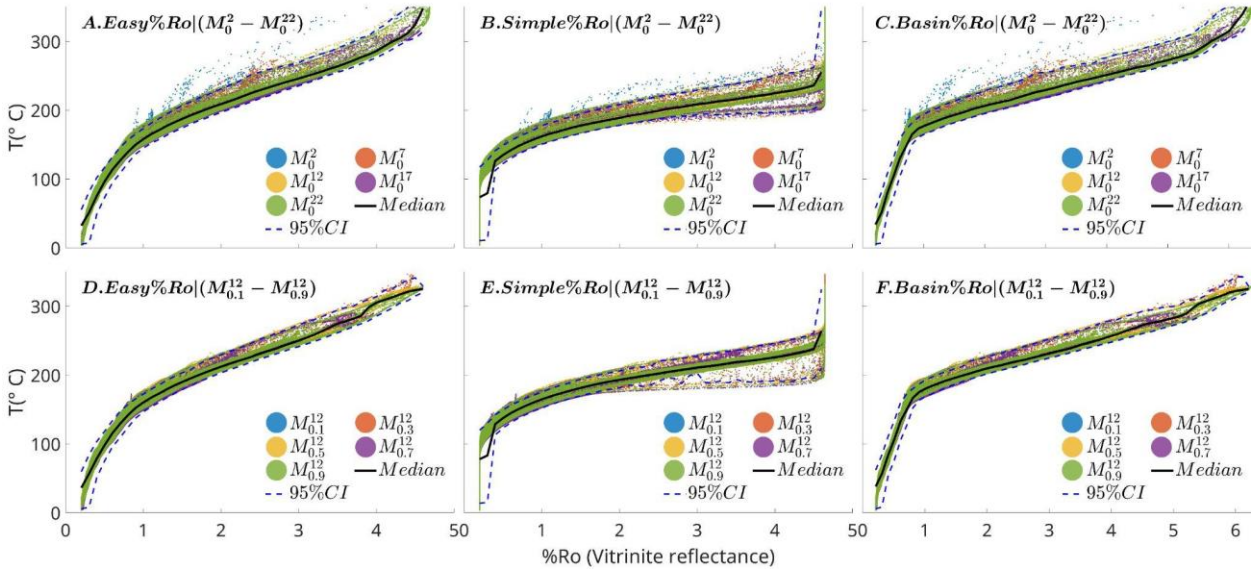

204

205

206 ***Fig. S7: %R₀** vs T for model(shown by smaller markers) and C0002 borehole(shown by large circular markers)*
207 *(Fukuchi et al., 2017).*

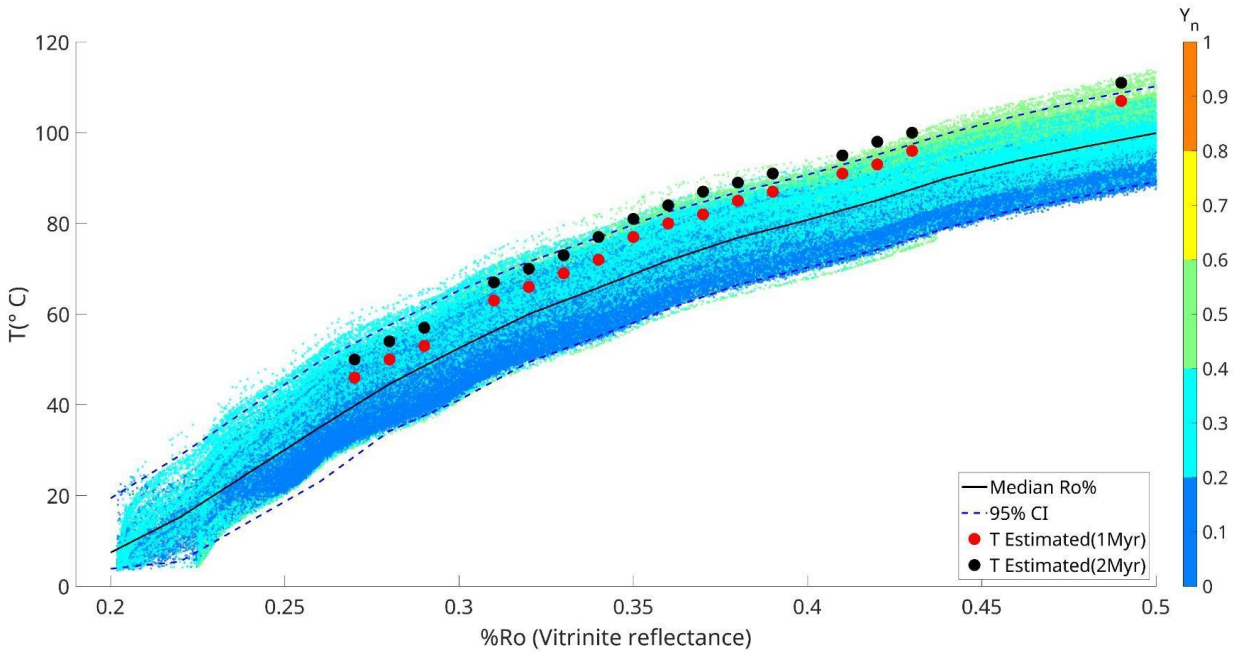

208

209

210